Clonal heterogeneity of acute myeloid leukemia treated with the IDH2 inhibitor Enasidenib

Lynn Quek[1,2,3*], Muriel D. David[4*], Alison Kennedy[1,2], Marlen Metzner[1,2], Michael Amatangelo[5], Alan Shih[6], Bilyana Stoilova[1,2], Cyril Quivoron[4], Maël Heiblig[4], Christophe Willekens[4,7], Véronique Saada[4,7], Samar Alsafadi[15], MS Vijayabaskar[11], Andy Peniket[3], Oliver A Bernard[4], Sam Agresta[8], Katharine Yen[8], Kyle MacBeth[5], Eytan Stein[6], George S. Vassiliou[11,12,13,14], Ross Levine[6,9,10], Stephane De Botton[4,7*], Anjan Thakurta[5*], Virginie Penard-Lacronique[4*] and Paresh Vyas[1,2,3*]

[1]MRC Molecular Hematology Unit, WIMM, University of Oxford, UK; [2]Haematology Theme Oxford Biomedical Research Centre and [3]Department of Hematology, Oxford University Hospitals NHS Foundation Trust, UK; [4]INSERM U1170, Gustave Roussy, Université Paris-Saclay, Equipe labellissée Ligue Nationale Contre le Cancer Villejuif, France, [5]Celgene Corporation, Summit, New Jersey, USA; [6]Department of Medicine, Leukemia Service, Memorial Sloan Kettering Cancer Center, New York, USA; [7]Département d'Hématologie, Gustave Roussy, Université Paris-Saclay, Villejuif, France, [8]Agios Pharmaceuticals, Inc., Cambridge, Massachusetts, USA; [9]Center for Hematologic Malignancies, Memorial Sloan Kettering Cancer Center, New York, USA; [10]Human Oncology and Pathogenesis Program, Memorial Sloan Kettering Cancer Center, New York; USA. [11]Haematological Cancer Genetics, Wellcome Trust Sanger Institute, Hinxton, Cambridge, CB10 1SA, UK; [12]Department of Haematology, University of Cambridge, Cambridge CB2 0PT, UK; [13]Department of Haematology, Cambridge University Hospitals NHS Trust, Cambridge CB2 0QQ, UK; [14]Cancer Research UK Cambridge Institute, University of Cambridge, Robinson Way, Cambridge, CB2 0RE, UK; [15]Département de Recherche Translationnelle/ Inserm U830, Institut Curie, Université Paris Sciences et Lettres, Paris, France.

*These authors contributed equally to this work

Corresponding authors: Paresh Vyas (paresh.vyas@imm.ox.ac.uk), Lynn Quek (lynn.quek@imm.ox.ac.uk), Virginie Penard-Lacronique (virginie.penard-lacronique@inserm.fr), Stephane de Botton (stephane.debotton@gustaveroussy.fr) and Anjan Thakurta (athakurta@celgene.com)

Total words (main text) : 4473

Abstract 177 words

Running Title: Clonal Responses in IDH2 mutant AML

Mutations in the gene encoding isocitrate dehydrogenase 2 (*IDH2*) occur in several types of cancer, including acute myeloid leukemia (AML). In model systems, mutant IDH2 causes hematopoietic differentiation arrest. Enasidenib, a selective small-molecule inhibitor of mutant IDH2, produces a clinical response in 40% of treated relapsed/ refractory AML patients by promoting leukemic cell differentiation. Here, we studied the clonal basis of response and acquired resistance to enasidenib treatment. Using sequential patient samples, we determined the clonal structure of hematopoietic cell populations at different stages of differentiation. Pre-therapy IDH2 mutant clones showed variable differentiation arrest. Enasidenib treatment promoted hematopoietic differentiation from either terminal or ancestral mutant clones; less frequently, treatment promoted differentiation of non-mutant cells. Analysis of paired diagnosis/relapse samples did not identify second site mutations in *IDH2* at relapse. Instead, relapse arose by clonal evolution, or selection, of terminal or ancestral clones, highlighting multiple bypass pathways that could potentially be targeted to restore differentiation arrest. Mapping clonal structure in cell populations at different stages of differentiation during therapy illustrates how different clones respond and evolve during relapse.

Differentiation arrest is a common feature of many cancer cells. Though intratumoral clonal heterogeneity is well documented, we lack a detailed understanding of how the complement of driver mutations within a clone, contribute to differentiation arrest. Furthermore, though it is clear that genetic and functional, intratumoral heterogeneity helps determine clinical outcome to cancer therapy[1,2], few studies have investigated the relationship between clonal structure and therapy response, particularly for therapies targeting oncogenic epigenetic processes. With an average of 13 somatic mutations per patient, arranged in an limited number of clones[3], AML is simpler than most cancers from a genomic context, providing a potential paradigm to answer these questions.

Somatic mutations in conserved arginine residues R140 and R172 in *ISOCITRATE DEHYDROGENASE 2* (*IDH2*) occur in 15-25% of AML patients[4-6]. The mutant proteins have neomorphic activity producing R-2-hydroxyglutarate (2-HG) that competitively inhibits 〈-ketoglutarate-dependent enzymes including the TET family of 5-methylcytosine (5mC) hydroxylases and Jumonji-C domain histone demethylases[7,8]. This leads to DNA hypermethylation[9], increased repressive histone methylation[8] and impaired hematopoietic differentiation that is reversed by mutant IDH inhibition in model systems [8,10-12].

We recently showed that enasidenib (AG-221/CC-90007), a first-in-class, allosteric inhibitor of mutant IDH2 (mIDH2)[13], reduces serum 2-HG, reverses DNA hypermethylation and promotes hematopoietic differentiation in preclinical models[13,14]. In a phase 1/2 clinical trial, enasidenib monotherapy produced a response rate of 40.3% in relapsed/refractory AML patients[15]. In most responding patients terminally mature blood cells were *IDH2* mutant, consistent with response due to enasidenib-induced differentiation of *IDH2* mutant cells[16]. However, in 9/71 (12.6%) responding patients, *IDH2* mutant cells were eliminated from peripheral blood cells[16]. Failure to respond to enasidenib was associated with a higher co-mutational burden and *NRAS* mutations[16]. Finally, most patients who initially responded eventually relapsed. These initial studies did not assess which clone(s) differentiated in response to enasidenib and the clonal mechanism of acquired enasidenib resistance.

We have addressed these two questions by studying sequential samples from a subset of trial patients. We showed marked variation in the degree of differentiation arrest of mutant *IDH2* clones. Restoration of differentiation by inhibition of mutant *IDH2* was also clone dependent, varying between patients, arising from either ancestral or terminal clones. In a minority of patients differentiation occurred from wild type progenitor cells, consistent with molecular remission in a subset of patient. Acquired resistance to enasidenib leading to differentiation arrest and relapse did not occur by second site mutations in *IDH2*. Instead, differentiation arrest was restored by multiple mechanisms through clonal evolution or clonal selection.

Results

Patient cohort studied

The trial enrolled 176 relapsed/refractory *IDH2* mutant AML patients[15]. Here, we studied a cytogenetically and genetically representative subset of 37 patients enriched for enasidenib responders (30/37 responders, **Supplementary Fig. 1a-c**). An extended mutational profile was determined in 33/37 patients by either whole exome sequencing (WES) (16/36 patients at read depth of 19-843x, average 121x at loci where variants were called), or targeted resequencing (17/36 patients) (**Supplementary Tables 1 and 2**). Compared to the entire trial cohort, the patient cohort studied here had similar serum baseline 2-HG levels and the mean level of 2-HG suppression was similar in the two cohorts (i.e. on-target response to enasidenib; **Supplementary Fig. 1d-e**).

Enasidenib rebalanced progenitor and precursor compartment sizes and restored progenitor function

In AML there are two orthogonal potential hierarchies (**Supplementary Fig. 2a**). There is clonal hierarchy with an initiating clone, transitional and terminal clones. We refer to all non-terminal clones as ancestral clones. These mutant clones exist in a second hierarchy, a hematopoietic cell hierarchy. AML initiating mutations occur in stem, or long-lived progenitor, cells but initiating clones are not usually arrested in differentiation[17-19]. However, with

acquisition of additional, transforming mutations and epigenetic alterations, clones fail to complete maturation. In the fully transformed state, haemopoiesis in human AML is dominated by expansion either of progenitor-like cells, presumably because of a differentiation block between progenitor and downstream precursor cells[20], or less commonly, by precursor-like cells, presumably because of a differentiation block between precursor and mature cells[21]. In both cases, expanded leukemic progenitor-like, or precursor-like, populations have functional leukemic stem cell activity[20,21]. Thus, we set out to address three questions: (i) where are individual clones arrested in the hematopoietic hierarchy; (ii) which clone(s) responded to mutant IDH2 inhibition by differentiating; (iii) which clone(s) were responsible for loss of response to enasidenib, after an initial response, and by what mechanism?

The experimental approach is set out in **Supplementary Fig. 2b**. We first performed flow cytometric quantitation of hematopoietic stem/progenitor ($Lin^-CD34^+CD117^+$), precursor ($Lin^-CD34^-CD117^+$) and mature myeloid cell ($Lin^-CD34^-CD117^-$) populations[21] at trial entry in 15 patients (**Fig. 1a-b and Supplementary Fig. 3a-b**). Sizes of individual stem/progenitor populations within Lin^-CD34^+ cells were also quantitated. 11/15 patients had abnormally expanded progenitor-like compartments (mainly LMPP-like and GMP-like; termed progenitor AML) and 4/15 abnormally large myeloid precursor-like populations (termed precursor AML). The ratio of progenitor: precursor AML is consistent with previous studies[20,21]**.**

Next, we analysed the bone marrow (BM) stem/progenitor/precursor populations in 5 patients who achieved complete remission (CR) with enasidenib (**Fig. 1b-c**). In all 5 there was near normalization of the sizes of the stem/progenitor compartments. Pre-treatment, 2 patients had pathologically expanded LMPP- and GMP-like progenitor populations (#201-023, #201-011) and 2 patients had expanded myeloid precursor compartments (#201-010 and #203-002). Functionally, Lin^-CD34^+ progenitor cells from these 5 patients in CR formed myeloid/ erythroid colonies nearly as efficiently as normal cells, in contrast to cells from patients who did not achieve CR (**Fig. 1d**)(**Supplementary Fig. 3c-d**). Thus, enasidenib

therapy rebalanced the sizes of hematopoietic stem/progenitor/precursor/mature populations at CR with reacquisition of normal myeloid progenitor function.

Wild type hemopoiesis occurs occasionally with enasidenib therapy

Next, we investigated the clonal basis of differentiation. In principle, enasidenib could have, directly or indirectly, restored differentiation from either wild type cells, ancestral clones or terminal clones in a clonal hierarchy (**Fig. 2a**). We established the clonal basis of response in 6 patients using samples taken at multiple time points before and through treatment, including relapse (**Fig. 2b**). We used WES and karyotype of bone marrow mononuclear cells (BMMNCs) to determine chromosomal copy number and mutational changes (**Supplementary Tables 2-3)**. Next, we used WES data to design patient-specific mutation panels to test variant allele frequencies (VAFs) of mutations in unsorted BMMNCs and flow-cytometric sorted hematopoietic stem/progenitor/precursor/mature cell populations and genotype flow-cytometric sorted single cells and hematopoietic colonies derived from single cells (**Supplementary Table 3**). A combination of all these data was used to establish clonal structures. Details on setting false positive and negative thresholds in single cell genotyping (SCG) are presented in Methods.

In our initial study, 9 out of 29 patients who achieved CR, for whom samples were available, had loss of mutant *IDH2* peripheral blood cells (complete molecular remission in peripheral blood[16]. However, it was unclear if these differentiated blood cells were truly wild type, or from a genetically mutant clone(s) that just lacked mutant *IDH2*? We studied this question in a patient with mutations in *IDH2 (I)*, *PEX26 (P)*, *FEZ2 S208T (F)*, *DNMT3B (D)*, *ZCCHC1 (Z)*, *NPM1 (N)*, and *ELMO3 (E)* in AML blasts pre-enasidenib (#201-022, **Fig. 2c**) who achieved mutant *IDH2* molecular remission. Pre-therapy, imputation from variant allele frequency (VAF) suggested presence of wildtype cells and three possible mutant clones: a clone with *IDH2* mutation alone (*I*), a clone with genotype *IPFDZN* and a minor clone that was either *IPFDZNE* or *IE* (**Supplementary Fig. 4a-c**), though the exact clonal structure could not established unambiguously (**Supplementary Fig. 4d-h**). At CR, the VAF of all

mutations was <1.6% (**Fig. 2c, Supplementary Table 4 for depth of sequencing**). Concordantly, at CR the majority (94.6%) of 111 individually genotyped hematopoietic colonies did not contain any mutations present pre-therapy (**Fig. 2d**). Functionally, the colonies produced a normal ratio of myeloid to erythroid colonies consistent with a wild-type genotype (**Fig. 2e**). Thus, in a minority of patients, enasidenib therapy resulted in restoration of wild type terminal blood cell production and progenitor function from wild-type cells.

Enasidenib restored differentiation from ancestral and terminal clones in a clone dependent manner

In one patient enasidenib promoted differentiation from an ancestral clone (#201-023, **Fig. 3**). WES and targeted resequencing of BMMNCs pre-enasidenib detected mutations in *SRSF2* (S), *IDH2* (I), *ASXL1* (A), *GATA2* (G) and two mutations in *RUNX1* (R, r) (**Supplementary Tables 2-3**). Pre-therapy imputation of clonal structure based on VAF in unsorted BMMNCs by exome and targeted resequencing suggested initial acquisition of *SRSF2* mutation (clone S) followed by an *IDH2* mutation (clone SI) followed by acquisition of *ASXL1* (*A*), the two *RUNX1* and *GATA2* mutations (**Supplementary Fig. 5a and Supplementary Tables 2-3**). At CR, only mutations *SRSF2* (S), *IDH2* (I), *ASXL1* (A) were detected in mature cells supporting the existence of an SIA clone that preferentially completes terminal maturation in presence of enasidenib (**Supplementary Fig. 5a-c)**.

To clarify clonal structure, and position clones within the haemopoietic hierarchy, we performed targeted resequencing for driver variants in 63 single cells and cell populations, from flow-cytometric sorted progenitor and mature myeloid cell compartments, from both pre-therapy and CR samples (**Fig. 3a-b and Supplementary Table 3**). This confirmed a linear clonal evolution pattern: clone SI preceded clone SIA, followed by clones that sequential acquired *RUNX1* mutations (clones SIAR and SIARr) and finally the terminal clone acquired a *GATA2* mutation (SIARrG). The mutational profile in 4 single cells did not fit into this clonal evolution pathway. We detected a single cell with an *ASXL1* mutation (clone A) and three single cells with both *ASXL1* and *SRSF2* mutations (clone AS). In three cells

with genotype AS, we detected allele dropout (ADO) of the *IDH2* allele in two out of three cells. Thus, we are unable to determine the mutational state of *IDH2* in those two cells. In contrast, in twelve cells of the SI clone, ADO of the *ASXL1* allele was detected in only three out of twelve cells (**Supplemental Fig. 12a**). Thus, though our results do not exclude a rarer, parallel clonal evolution pathway where clones A and AS exist and failed to acquire mutations in the order shown in the main pathway, they also are consistent with these cells being part of the main clonal evolution pathway.

Pre-therapy, 90% of BMMNCs were progenitors (LMPP and GMP) (**Fig. 1c and 3d)** and 90-100% of these leukemic progenitors were the SIARrG clone (**Fig 3c**). Thus, the SIARrG clone is arrested in differentiation at the progenitor stage and expands to dominate the marrow. Less than 10% of BMMNCs were mature myeloid cells (**Fig 1c** and **Fig 3d**). We were only able to genotype 8 mature myeloid cells pre-therapy (**Fig. 3c**) and they are composed of a mixture of wild type cells and of cells with genotypes A, SI, AS and SIA. At CR, the mature myeloid cell compartment comprised 60% of BMMNCs (**Fig 1c** and **Fig 3d**) and 85% of mature cells have the *SIA* genotype (**Fig. 3d** and **Supplementary Fig. 5b, Supplementary Table 3**).

The progenitor compartment was only 20% of BMMNCs at CR (**Fig. 1c and Fig 3d**) and composed of mixed ancestral clones SI, SIA, SIAR but not the terminal clone SIARrG. Concordantly, the majority of colonies generated by progenitors at CR were “SIA”, with a minority of the SI and SIA genotype (**Fig. 3e**). The ratio of myeloid:erythroid colonies was within normal limits (**Fig. 3f**) Taken together, this data demonstrated a complex, clone-dependent pattern of enasidenib-induced differentiation with mature myeloid cell production sustained principally by a self-renewing ancestral *SIA* clone.

In four patients, differentiation of mature cells was principally seen from terminal clones (**Fig. 2b**). In patient #201-011, WES (**Supplementary Table 2**) and targeted resequencing of BMMNC revealed two mutations in *DNMT3A* and mutations in *IDH2*, *ASXL1* and *XPO1* pre-therapy that persisted at different VAFs at CR (**Supplementary Table 3**, **Supplementary**

Fig. 6a). However, it was not possible to impute the clonal structure from the VAF (**Supplementary Fig. 6b**). We genotyped 110 single cells, pre-therapy and at CR (**Fig. 4a**). This revealed an initiating *DNMT3A* clone *(*clone D) that acquired an *IDH2* mutation (clone DI) (**Fig. 4b**). Subsequently, there is a branching clonal structure with two terminal clones; one acquired an *XPO1* mutation (clone DIX), whereas the other acquired two mutations, a second *DNMT3A* mutation and an *ASXL1* mutation (clone DIdA). SCG suggested the DIdA clone may have arisen by convergent evolution through intermediate DId and DIA clones. There is a caveat with this interpretation as ADO was detected in 6 out of 7 DIA clone cells (**Supplemental Fig. 12d**). In the DId cells, though there were no heterozygous germline single nucleotide polymorphisms in the *ASXL1* gene, the estimated ADO frequency of the *ASXL1* allele was 12.1% (**Supplemental Fig. 12e**). Thus, it is also possible that the DIdA clone may also have arisen through just one mutational pathway.

Pre-enasidenib, 89% of BMMNCs were leukemic progenitors (LMPP and GMP) virtually exclusively composed of the DIX clone (**Fig. 4c-d**). A small mature myeloid population is present pre-enasidenib composed of the DIdA clone (**Supplementary Fig. 6c**). These observations suggest that the *IDH2* mutation in the context of the DIdA clone is not fully effective at imposing a complete differentiation block, whereas the same *IDH2* mutation in the context of the DIX clone fully arrests at a progenitor stage.

At CR, 82% of BMMNCs were composed of mature myeloid cells, 85% of which were a mix of two terminal branching clones DIdA (54%) and DIX (31%) suggesting enasidenib promoted differentiation from both terminal clones (**Fig. 4c-d, Supplementary Table 3**). To address which progenitors contribute to mature cell output we genotyped single flow cytometric sorted progenitors. The DIdA clone dominated mature GMP, CMP and MEP progenitor compartments (**Fig. 4c-d**). In contrast, clone DIX was detected only in the more immature LMPP progenitor compartment. GMP, CMP and MEP are more clonogenic than the LMPP[20,22] and concordantly, ~95% of colonies had the DIdA genotype (**Fig. 4e**) that were myeloid-biased (**Fig. 4f**). Interestingly, there is a substantial decrease in the size of the

LMPP compartment at CR compared to pre-therapy (**Fig. 4d**) (1240-fold decrease within the Lin^- compartment and 81-fold within the $CD34^+$ compartment).

In three additional patients the terminal clone contributed to mature myeloid cells at CR based on imputed clonal structures, genetic analysis of mature myeloid cells at CR (patient #201-010, **Supplementary Fig. 6d-e**) and genotyping of myeloid colonies at CR (patient #201-027, **Supplementary Fig. 7a-d**; patient #201-006 **Supplementary Fig. 7e-h**). Depth of coverage for each of the mutations in all three patients is in **Supplementary Table 4**.

In summary, enasidenib therapy provides relief of differentiation arrest at a progenitor-like or precursor-like stage, normalizing the sizes of these abnormally expanded compartments. The ability of mutant *IDH2* to impose differentiation block is dependent on the context of co-associated mutations within a clone. Consequently, efficacy of enasidenib-induced differentiation is also is likely to dependent mutational landscape within a clone.

Relapse of IDH2 mutant patients on enasidenib occurs by clonal selection/evolution and not second site mutations in *IDH2* gene

Although responding patients have a median survival of 18-21 months, many patients relapse[15]. To study mechanisms leading to relapse we measured 2-HG levels in 16 patients at diagnosis and relapse, mutational profiles in 12 patients (by WES in 11 cases and targeted sequencing in the other patient) and performed karyotype analysis in 11 subjects (**Fig. 5a-b** and **Supplementary Table 5**). We did not detect second site *IDH2* mutations at relapse in any patient but instead documented 7 patterns of clonal evolution/selection with acquisition of recurrent AML-associated genetic changes (**Fig. 5a**). These are recurrent missense mutations in myeloid malignancy, or nonsense and frameshift mutations in cancers, as documented in the COSMIC database (http://cancer.sanger.ac.uk/cosmic). For patient #201-007, mutations were detected prior to relapse, but increased in frequency at relapse (Supplementary Table 3).

In 14/16 patients 2-HG levels remained suppressed between best response (CR or PR) and relapse suggesting drug was on target in suppressing neomorphic enzyme function (**Fig. 5b**). However, in 2 patients (#201-014 and #201-022) rising 2-HG levels and BM leukemic cells (blasts) were seen (**Fig. 5c-d**). Exome sequencing revealed *IDH1* R132C/H mutations albeit accompanied by other genetic abnormalities, some of which are recurrent in AML (point mutations in *RUNX1*, *NPM1 and* t(3:12)) (**Fig. 5e-f**). These *IDH1* mutations were previously undetectable by high depth NGS (10000x) pre-enasidenib therapy. Surprisingly, in both cases, the VAF indicates that *IDH1* mutations were present in *IDH2* mutant clones.

Relapse also associated with increasing VAF of oncogenic gain of function mutations in genes encoding cytokine receptors *CSF3R* (patient #104-021, **Supplementary Fig. 8a-b**) and *FLT3* (patients #201-013, #201-004 **Supplementary Fig. 8c-d** and #201-007 **Supplementary Fig. 9f-h**) and predicted loss of function mutation in the negative regulator of cytokine signalling *CBL* (#201-004 **Supplementary Fig. 8d**). For patient #104-021 we could not resolve the clonal structure from targeted resequencing of BMMNC (**Supplementary Fig. 8b**, **Supplementary Table 2)** but genotyping of 214 single cells pre-enasidenib and at relapse (**Fig. 6a**) demonstrated an initiating *DNMT3A*/ *IDH2* mutant clone that spawned the major clone with a recurrent *U2AF1* mutation (DIU clone). A minor DIUF clone with a D200E variant in the *FLT3* (not previously described in AML) was also present pre-enasidenib. At relapse, the major clone in the expanded arrested LMPP and GMP compartments had acquired an oncogenic T618I mutation in the cytokine receptor *CSF3R* that is well described in myeloid leukemias[23] (*DIUC clone*). DIUC further evolved, acquiring a variant in *NFKB1* that has not been described previously in AML. Mutations in both *CSF3R* and *NFKB1* were detectable at threshold of sensitivity pre-enasidenib (**Supplementary Fig. 8a**).

Relapse, and re-imposition of differentiation block, was also associated with previously described mutations in hematopoietic transcription factors in myeloid cancers. These included frame shift mutations in *RUNX1* (**Fig. 5e and Supplementary Fig. 8e** one of which

has been previously described in AML (*RUNX1* F416fs) [24]) and *BCORL1*[25]; non-synonymous variants, in the DNA- and protein-partner binding N-terminal zinc finger of *GATA2* (**Supplementary Fig. 8d**)[26,27] and in one of the zinc fingers of *BCL11A*[28] **(Supplementary Fig. 8c**). In all patients these mutations were not detected pre-enasidenib.

Deletion of all (monosomy 7), or part (del 7q) of chromosome 7 is common in myeloid malignancy[29]. Chromosomal abnormalities were present in 18% of the enasidenib cohort[15] and 20% in the cohort studied here (**Supplementary Fig 1**). Del 7q was detected in 4 out of 12 patients who relapsed (#201-010, #201-007, #201-019 and #201-003) (**Fig. 5a, Supplementary Table 5**) but are not enriched in relapsed patients (Amatangelo, M., Thakurta, A., unpublished data). In all four patients it was detected either cytogenetically, or by WES, pre-enasidenib therapy (**Supplementary Tables 2 and 5**). In three out of the four cases the del 7q clone was selected at relapse (**Supplementary Fig. 9a-e**, **k** and **l**). In one case where it was not, it was the dominant clone pre-therapy and at relapse (**Supplementary Fig. 9g-j**).

Clonal evolution at relapse also highlighted variants in genes less well studied in AML including *NFKB1* M216I (**Fig. 6a-d**), *DDX1* G699A (**Supplementary Fig. 8c**), *MTUS1* Q781H (**Supplementary Fig. 9f-i**), *DHX15* R222G and *DEAF1* N372K (**Fig. 6e-h**). Of these, acquisition of latter two variants by patient #201-011 at relapse is worthy of comment. Pre-enasidenib the patient had expanded LMPP and GMP populations composed of an arrested DIX clone (**Fig. 4b**). At CR the DIX clone was able to differentiate but only persisted within the LMPP compartment (**Fig. 4d**). At relapse, we detected 30 cells with DIX mutations that acquired a missense mutation in the DExD/H-box helicase *DHX15* R222G (mutation H), 7 cells with the DIX mutations that had acquired a variant in the transcription factor *DEAF1* N372L (variant F) and 12 cells with the DIXHF variants (**Fig. 6e-f**). However in 6 out of 7 DIXF cells there was ADO for the *DHX15* allele with the *DHX15* R222G mutation and therefore we are unable to determine whether the *DHX15* R222G is present in those cells (**Supplementary Fig. 12c**).

Acquisition of the additional *DHX15* and *DEAF1* mutations was associated with differentiation arrest, and a re-expansion of LMPP and GMP progenitor compartments, comprising 89% of MNCs. 83% of LMPP cells were composed of the DIXH and DIXHF clones whereas in the GMP-like compartment there was a more even contribution by the *DIXHF*, *DIXH* and *DIXF* clones (**Fig. 6g-h**).

Finally, both DHX15 and DDX1 regulate RNA splicing. Human DHX15 is structurally closely related to its yeast homologue, Prp43[30,31]. Both proteins have been shown to contribute to disassembly of splicesomes, efficient debranching and turnover of excised introns[32,33]. *DHX15* R222G mutations have been previously described in AML[34,35]. To determine if acquisition of *DHX15* R222G results in altered splicing we performed RNA-Seq of AML blasts at relapse from patient #201-011 and compared splicing to AML cells from the same patient that were wild type for DHX15 at trial entry (**Supplementary Fig. 8f**). In cells expressing *DHX15* R222G, there were alterations in exon skipping and intron retention compared to cells wild type for *DHX15*. DDX1 is a DEAD-box RNA helicase with 5' single stranded RNA exonuclease activity postulated to have multiple roles in RNA metabolism[36]. *DDX1* G699A has not been previously described as a cancer-associated mutation nor has its impact on RNA splicing been studied. Our data shows an increase in intron retention and use of alternative 5' and 3' splice sites, and a decrease in spliced exons in mutant compared to wild type AML cells from the same patient (**Supplementary Fig. 8g**).

Discussion

This study of clonal response and acquired resistance in sequential paired samples from AML patients treated with an IDH2 inhibitor extends prior preclinical studies[13,14]. Pre-enasidenib there were complex patient- and clone-specific patterns of differentiation arrest. At CR, wildtype dominated cellular reconstitution was less common but does occur. More commonly, enasidenib causes a clone-specific differentiation response, either from ancestral or terminal clones, leading to near normalization of the sizes and functionality of progenitor and precursor hematopoietic compartments with altered clonal mix. Acquired resistance was

never due to a second site mutation in the same *IDH2* allele but instead due to either clonal evolution or clonal selection. At least 7 different mutational mechanisms led to re-imposition of differentiation arrest (**Supplementary Fig.10**).

In most patients enasidenib was unable to promote terminal differentiation and eradication of IDH2 mutant clones; ancestral and/or terminal clones remained at CR. In patients with restitution of wild type hemopoiesis, we infer that enasidenib most likely promoted terminal differentiation of arrested self-renewing IDH2 mutant cells, allowing normal cells to dominate hemopoiesis. Longer term clinical follow up of molecular CR patients will determine if molecular CR patients have a better clinical outcome and if they relapse, the clonal origin of relapse. More generally, understanding the molecular mechanisms of relief from differentiation arrest by IDH2 inhibitors will require in depth study of changing patterns of epigenetic marks and transcriptional programmes within highly purified, clone-specific, hematopoietic stem, progenitor and precursor populations, before and after drug exposure, as transcriptional and epigenetic profiles are so highly plastic through differentiation.

Drug resistance to targeted cancer therapy arises by multiple mechanisms. Resistance to kinase inhibitors in AML[37,38], chronic myeloid leukemia[39], chronic lymphoid leukemia[40] and lung cancer[41,42] often involves second site mutations in the mutant allele modulating drug or substrate binding or copy number changes of the mutant kinase. We did not observe this in enasidenib treated patients.

Acquired resistance led to IDH2 could arise by either epigenetic or genetic mechanisms or a combination of the two. In most patients 2HG remained suppressed at relapse suggesting that enasidenib remained on target and relapsed clones were not dependent on mutant IDH2. In hematologic malignancies, genome-wide epigenetic variation (DNA methylation for example) can be several orders more variable than genetic change[43-45], is somatically heritable, and subject to selection. Locus-specific DNA methylation (epiallele) variation shows dynamic change in AML between diagnosis and relapse and can occur with distinct kinetics, such that some patients have a high epiallele diversity and low somatic mutation

burden and vice versa[45]. In melanoma, resistance to a B-RAF inhibitor arose in rare cells through stochastic, transient variation in gene expression that was selected for by therapy[46]. This is consistent with prior work on chromatin mediated drug resistance in cancer cell lines[47].

Clones acquiring gene mutations, or grosser genetic changes, have previously been reported in therapy resistant chronic lymphocytic leukemia[48] and medulloblastoma[49]. Acquisition of an *IDH1* mutation in two patients is an example of how this may occur. Here, these AML propagation is likely to be highly dependent to high 2HG. 2HG addiction may be AML cell autonomous or alternatively, the 2HG requirement may be in BM niche supporting cells or other non-AML cell populations. AML clone-specific and non-AML cell specific analysis of the impact of 2HG on epigenetic and transcriptional programs and metabolism of cells[50] is needed to understand this dependency. Other examples genetic changes leading to enasidenib resistance include gain of function mutations in proliferative cytokine signalling pathways and loss of or altered function in transcriptional regulators of hemopoiesis. However, mutations in the RAS pathway that are correlate with failure of initial response[16] were not associated with acquired resistance.

We also detected variants at relapse not previously well studied in AML. An example of this is the *DHX15* R222G mutation, recently described in *RUNX1-RUNXT1* AML[34]. The yeast homologue of DHX15, Prp43, regulates RNA splicing and ribosome biogenesis. Loss of wild type DHX15 and overexpression of mutant DHX15 increases alternative splicing. In contrast, a role for DEAF1 has not been previously published in normal or malignant hemopoiesis. Curiously DEAF1 is a paralog of the transcription factor, RUNXT1. DEAF1 is expressed throughout hemopoiesis but particularly in GMP and AML blasts[21]. In non-hemopoetic tissues it binds to LMO4, a member of the LMO transcriptional adapter protein family. In blood cells, LMO2, a closely related LMO family member, partners transcription factors including GATA, E-box proteins and LDB1 to form regulatory and oncogenic protein complexes. Thus, the role of DEAF1 in hemopoiesis and its interaction with DHX15 merits

401 further study. More broadly, a deeper mechanistic understanding of how wild-type IDH2
402 promote hematopoietic differentiation, which is currently poorly understood, will also
403 increase our understanding of how bypass pathways could re-impose differentiation block,
404 for example by altering transcriptional programmes, as seen in BET inhibitor therapy
405 resistance[51].

406 Finally, this study demonstrates how any cancer therapy alters clonal structure across a fully
407 transformed and pre-malignant cellular hierarchy. By defining clonal structures and mapping
408 where clones were arrested across differentiation, in purified hematopoietic compartments,
409 we obtained a previously unavailable view of where different clones were arrested. This
410 provides the necessary information to study why clones are arrested at different stages of
411 differentiation. Furthermore, analysis of sequential samples through therapy shows how
412 clones differentially responded to therapy. This provides the basis to study clone specific
413 relief of IDH2 inhibition. More generally, our approach could be applied to any cancer
414 therapy, where single cell suspensions and purification of cells at different stages of
415 differentiation is possible. This would then provide a clone specific understanding of how
416 therapy alters clonal structure through a cellular hierarchy. Our approach also provides
417 insights towards a rational basis for combination therapies to reduce drug resistance.

418 **Acknowledgments:** We thank patients and clinical staff for samples studied. L.Q. was
419 supported by an Oxford-Celgene Fellowship; P.V. acknowledges funding from the MRC
420 Disease Team Awards (G1000729/94931 and MR/L008963/1) MRC Molecular Haematology
421 Unit and the Oxford Partnership Comprehensive Biomedical Research Centre (NIHR BRC
422 Funding scheme. oxfbrc-2012-1). V.P.-L. and S.dB. acknowledge funding by the French
423 National Institute of Health (INSERM-AVIESAN), the National Cancer Institute (INCa-DGOS-
424 Inserm_6043 and INCa 2012-1-RT-09), SIRIC-SOCRATE 2.0 and the Fondation Association
425 pour la Recherche sur le Cancer (ARC, Programme). M.D.D. is funded by a fellowship from
426 the Institut National du Cancer (INCa-DGOS_5733). M.H. is a fellow of the Fondation
427 Philanthropia, Ecole des Sciences du Cancer, Gustave Roussy, Villejuif, France. We

428 acknowledge the Core Flow Cytometry and Next Generation Sequencing Facilities at the
429 WIMM; the Imaging, Cytometry and Integrated Biology platforms at Gustave Roussy
430 (Philippe Rameau, Yann Lecluse, Nathalie Droin, M'boyba Khadija Diop, UMS AMMICa);
431 clinical departments at Gustave Roussy (Jean-Baptiste Micol for clinical specimens, Nathalie
432 Auger for cytogenetic analyses and Christophe Marzac and Edwidge Leclercq for FLT3
433 genotyping) and Memorial Sloan Kettering. R.L.L. is supported by grants from the NIH,
434 including R35 CA197594-01A1 and the Memorial Sloan Kettering Cancer Center Support
435 Grant (NIH P30 CA008748, including a supplement to R.L.L.). The views expressed are
436 those of the authors and not necessarily those of the NHS, the NIHR or the Department of
437 Health.

438 **Author contributions**:

439 L.Q., M.D.D. designed/ performed experiments, analysed data; A.K., M.M., M.A., B.S., C.Q.,
440 M.H., C.W., V.S., S.Al. performed experiments/ analysed data; M.S.V. and G.S.V. analysed
441 data; M.A., A.S., A.P., K.Y., S.Ag., S.dB., R.L.L., E.S., K.M., A.T. provided
442 reagents/samples/clinical data; O.A.B., S.dB., A.T., R.L.L., V.P.-L. and P.V. designed the
443 experiments/ analysed the data. L.Q. and P.V. wrote the manuscript. All authors edited the
444 manuscript.

445

446 **Competing interests**:

447 PV has received research grant support from Celgene and is on its speaker bureau. LQ has
448 received research grant support from Celgene

449 **Data and materials availability**: Exome sequencing data has been deposited in
450 ArrayExpress under accession E-MTAB-6299. RNA sequencing data has been deposited in
451 ArrayExpress under accession E-MTAB-6660.

452 **References**

453 1. Abbosh, C*., et al.* Phylogenetic ctDNA analysis depicts early-stage lung cancer
454 evolution. *Nature* **545**, 446-451 (2017).

2. Jamal-Hanjani, M.*, et al.* Tracking the Evolution of Non-Small-Cell Lung Cancer. *N Engl J Med* **376**, 2109-2121 (2017).
3. Cancer Genome Atlas Research, N. Genomic and epigenomic landscapes of adult de novo acute myeloid leukemia. *N Engl J Med* **368**, 2059-2074 (2013).
4. Paschka, P.*, et al.* IDH1 and IDH2 mutations are frequent genetic alterations in acute myeloid leukemia and confer adverse prognosis in cytogenetically normal acute myeloid leukemia with NPM1 mutation without FLT3 internal tandem duplication. *J Clin Oncol* **28**, 3636-3643 (2010).
5. Green, C.L.*, et al.* The prognostic significance of IDH2 mutations in AML depends on the location of the mutation. *Blood* **118**, 409-412 (2011).
6. Craddock, C.F.*, et al.* Outcome of Azacitidine Therapy in Acute Myeloid Leukemia Is not Improved by Concurrent Vorinostat Therapy but Is Predicted by a Diagnostic Molecular Signature. *Clin Cancer Res* (2017).
7. Xu, W.*, et al.* Oncometabolite 2-hydroxyglutarate is a competitive inhibitor of alpha-ketoglutarate-dependent dioxygenases. *Cancer Cell* **19**, 17-30 (2011).
8. Lu, C.*, et al.* IDH mutation impairs histone demethylation and results in a block to cell differentiation. *Nature* **483**, 474-478 (2012).
9. Figueroa, M.E.*, et al.* Leukemic IDH1 and IDH2 mutations result in a hypermethylation phenotype, disrupt TET2 function, and impair hematopoietic differentiation. *Cancer Cell* **18**, 553-567 (2010).
10. Losman, J.A.*, et al.* (R)-2-hydroxyglutarate is sufficient to promote leukemogenesis and its effects are reversible. *Science* **339**, 1621-1625 (2013).
11. Wang, F.*, et al.* Targeted inhibition of mutant IDH2 in leukemia cells induces cellular differentiation. *Science* **340**, 622-626 (2013).
12. Kats, L.M.*, et al.* Proto-oncogenic role of mutant IDH2 in leukemia initiation and maintenance. *Cell Stem Cell* **14**, 329-341 (2014).
13. Yen, K.*, et al.* AG-221, a First-in-Class Therapy Targeting Acute Myeloid Leukemia Harboring Oncogenic IDH2 Mutations. *Cancer discovery* **7**, 478-493 (2017).

14. Shih, A.H., *et al.* Combination Targeted Therapy to Disrupt Aberrant Oncogenic Signaling and Reverse Epigenetic Dysfunction in IDH2- and TET2-Mutant Acute Myeloid Leukemia. *Cancer discovery* **7**, 494-505 (2017).
15. Stein, E.M., *et al.* Enasidenib in mutant IDH2 relapsed or refractory acute myeloid leukemia. *Blood* **130**, 722-731 (2017).
16. Amatangelo, M.D., *et al.* Enasidenib induces acute myeloid leukemia cell differentiation to promote clinical response. *Blood* **130**, 732-741 (2017).
17. Jan, M., *et al.* Clonal evolution of preleukemic hematopoietic stem cells precedes human acute myeloid leukemia. *Sci Transl Med* **4**, 149ra118 (2012).
18. Corces-Zimmerman, M.R., Hong, W.J., Weissman, I.L., Medeiros, B.C. & Majeti, R. Preleukemic mutations in human acute myeloid leukemia affect epigenetic regulators and persist in remission. *Proc Natl Acad Sci U S A* **111**, 2548-2553 (2014).
19. Shlush, L.I., *et al.* Identification of pre-leukaemic haematopoietic stem cells in acute leukaemia. *Nature* **506**, 328-333 (2014).
20. Goardon, N., *et al.* Coexistence of LMPP-like and GMP-like leukemia stem cells in acute myeloid leukemia. *Cancer Cell* **19**, 138-152 (2011).
21. Quek, L., *et al.* Genetically distinct leukemic stem cells in human CD34- acute myeloid leukemia are arrested at a hemopoietic precursor-like stage. *J Exp Med* **213**, 1513-1535 (2016).
22. Karamitros, D., *et al.* Human lympho-myeloid progenitors are heterogeneous at the single cell level. *Nature Immunology* **19**, 85-97 (2018).
23. Maxson, J.E., *et al.* Oncogenic CSF3R mutations in chronic neutrophilic leukemia and atypical CML. *N Engl J Med* **368**, 1781-1790 (2013).
24. Gaidzik, V.I., *et al.* RUNX1 mutations in acute myeloid leukemia: results from a comprehensive genetic and clinical analysis from the AML study group. *J Clin Oncol* **29**, 1364-1372 (2011).
25. Li, M., *et al.* Somatic mutations in the transcriptional corepressor gene BCORL1 in adult acute myelogenous leukemia. *Blood* **118**, 5914-5917 (2011).

26. Papaemmanuil, E.*, et al.* Genomic Classification and Prognosis in Acute Myeloid Leukemia. *N Engl J Med* **374**, 2209-2221 (2016).
27. Fasan, A.*, et al.* GATA2 mutations are frequent in intermediate-risk karyotype AML with biallelic CEBPA mutations and are associated with favorable prognosis. *Leukemia* **27**, 482-485 (2013).
28. Mason, C.C.*, et al.* Age-related mutations and chronic myelomonocytic leukemia. *Leukemia* **30**, 906-913 (2016).
29. Grimwade, D.*, et al.* Refinement of cytogenetic classification in acute myeloid leukemia: determination of prognostic significance of rare recurring chromosomal abnormalities among 5876 younger adult patients treated in the United Kingdom Medical Research Council trials. *Blood* **116**, 354-365 (2010).
30. Tauchert, M.J., Fourmann, J.B., Luhrmann, R. & Ficner, R. Structural insights into the mechanism of the DEAH-box RNA helicase Prp43. *eLife* **6**(2017).
31. Murakami, K., Nakano, K., Shimizu, T. & Ohto, U. The crystal structure of human DEAH-box RNA helicase 15 reveals a domain organization of the mammalian DEAH/RHA family. *Acta Crystallogr F Struct Biol Commun* **73**, 347-355 (2017).
32. Arenas, J.E. & Abelson, J.N. Prp43: An RNA helicase-like factor involved in spliceosome disassembly. *Proc Natl Acad Sci U S A* **94**, 11798-11802 (1997).
33. Fourmann, J.B.*, et al.* Dissection of the factor requirements for spliceosome disassembly and the elucidation of its dissociation products using a purified splicing system. *Genes Dev* **27**, 413-428 (2013).
34. Faber, Z.J.*, et al.* The genomic landscape of core-binding factor acute myeloid leukemias. *Nat Genet* **48**, 1551-1556 (2016).
35. Farrar, J.E.*, et al.* Genomic Profiling of Pediatric Acute Myeloid Leukemia Reveals a Changing Mutational Landscape from Disease Diagnosis to Relapse. *Cancer Res* **76**, 2197-2205 (2016).
36. Cordin, O., Banroques, J., Tanner, N.K. & Linder, P. The DEAD-box protein family of RNA helicases. *Gene* **367**, 17-37 (2006).

37. Cools, J., *et al.* Prediction of resistance to small molecule FLT3 inhibitors: implications for molecularly targeted therapy of acute leukemia. *Cancer Res* **64**, 6385-6389 (2004).

38. Heidel, F., *et al.* Clinical resistance to the kinase inhibitor PKC412 in acute myeloid leukemia by mutation of Asn-676 in the FLT3 tyrosine kinase domain. *Blood* **107**, 293-300 (2006).

39. Shah, N.P., *et al.* Multiple BCR-ABL kinase domain mutations confer polyclonal resistance to the tyrosine kinase inhibitor imatinib (STI571) in chronic phase and blast crisis chronic myeloid leukemia. *Cancer Cell* **2**, 117-125 (2002).

40. Woyach, J.A., *et al.* Resistance mechanisms for the Bruton's tyrosine kinase inhibitor ibrutinib. *N Engl J Med* **370**, 2286-2294 (2014).

41. Kobayashi, S., *et al.* EGFR mutation and resistance of non-small-cell lung cancer to gefitinib. *N Engl J Med* **352**, 786-792 (2005).

42. Choi, Y.L., *et al.* EML4-ALK mutations in lung cancer that confer resistance to ALK inhibitors. *N Engl J Med* **363**, 1734-1739 (2010).

43. Figueroa, M.E., *et al.* DNA methylation signatures identify biologically distinct subtypes in acute myeloid leukemia. *Cancer Cell* **17**, 13-27 (2010).

44. Kulis, M., *et al.* Epigenomic analysis detects widespread gene-body DNA hypomethylation in chronic lymphocytic leukemia. *Nat Genet* **44**, 1236-1242 (2012).

45. Li, S., *et al.* Distinct evolution and dynamics of epigenetic and genetic heterogeneity in acute myeloid leukemia. *Nat Med* **22**, 792-799 (2016).

46. Shaffer, S.M., *et al.* Rare cell variability and drug-induced reprogramming as a mode of cancer drug resistance. *Nature* **546**, 431-435 (2017).

47. Sharma, S.V., *et al.* A chromatin-mediated reversible drug-tolerant state in cancer cell subpopulations. *Cell* **141**, 69-80 (2010).

48. Landau, D.A., *et al.* Evolution and impact of subclonal mutations in chronic lymphocytic leukemia. *Cell* **152**, 714-726 (2013).

49. Morrissy, A.S., *et al.* Divergent clonal selection dominates medulloblastoma at recurrence. *Nature* **529**, 351-357 (2016).

50. Raffel, S., *et al.* BCAT1 restricts alphaKG levels in AML stem cells leading to IDHmut-like DNA hypermethylation. *Nature* **551**, 384-388 (2017).

51. Rathert, P., *et al.* Transcriptional plasticity promotes primary and acquired resistance to BET inhibition. *Nature* **525**, 543-547 (2015).

Figure Legends

Figure 1. Enasidenib treatment induces differentiation of AML progenitor and precursor cell populations and restores progenitor function.

a) Top, immunophenotyping of hematopoietic stem/progenitor/precursor and mature cell populations in AML bone marrow (BM) samples pre-treatment showing expanded progenitor (n=11 biologically independent samples) or precursor (n=4 biologically independent samples) populations with normal BM (n=8 biologically independent samples). Below, detailed composition of stem/progenitor compartments in AML pre-treatment (n=15 biologically independent samples) and normal BM (n=12 biologically independent samples). Error bars in normal BM= 95% confidence interval. HSC: hematopoietic stem cell, MPP: multipotent progenitor, LMPP: lymphoid-primed multipotent progenitor, CMP: common myeloid progenitor, MEP; megakaryocyte-erythroid progenitor; GMP: granulocyte-macrophage progenitor.

b) Top, schematic representation of flow cytometric approach and sequential gates used to analyse samples in (a). Lin^-, lineage negative; BMMC, bone marrow mononuclear cells. Bottom, example of flow plots from a representative sample prior to enasidenib treatment (Pre-ENA) and at complete remission (CR) in patients with expanded progenitor-like populations (#201-023; left, experiment performed once) or expanded myeloid precursor-like population (#201-010; right, experiment performed once). Numbers shown within the gate indicate percentage of the corresponding cell population compared to all cells in the plot.

c) Top, immunophenotyping of hematopoietic cell populations in normal BM (left, as in (a)) and in samples from 5 patients (#201-023, #201-011, #201-022, #201-010, #203-002) pre-ENA, at intermediate time points during treatment, and at CR. Bottom, sizes of stem and progenitor compartments. Abbreviations and error bars in normal BM are as in (a). C=cycle, D=day.

d) Number of mixed erythroid-myeloid colonies (GEM), granulocyte-macrophage (GM), granulocyte (G), macrophage (M) and erythroid (E) colonies produced per 100 plated flow-sorted $CD34^+$ cells from normal BM (n=4 biologically independent samples), enasidenib-treated patients in CR (n=5 biologically independent samples) and enasidenib-treated patients not in CR (n=3 biologically independent samples). Patient samples were plated with addition of Enasidenib (1μM) to semi-solid media. Error bars= standard error of the mean. P-values determined by 2-sided Student's paired t-test.

Figure 2. Differentiation response arising from wild-type cells in patients treated with enasidenib.

a) Schematic representation of varying possible clonal responses to enasidenib. Four mutations (A, B, C and D) are present in four clones that are arranged in a branching structure. A differentiation response to enasidenib treatment could potentially occur from either wild type cells or from ancestral or terminal clones.

b) Summary of the type of differentiation response (from either wild type cells, ancestral or terminal clones) in samples from 6 patients.

c) Variant allele frequencies (VAF) of the indicated mutations in AML blasts of patient #201-022 prior to enasidenib treatment (Pre-ENA) and in peripheral blood mononuclear cells (PMNC) at CR, as assessed by targeted re-sequencing.

d) Clonal contribution to colony output from the CR sample from patient #201-022, as a percentage of all individually picked colonies genotyped. Clones were identified as wild type (WT), carrying the *FEZ2* P118S mutation (F), or carrying the *FEZ2* P118S and *DNMT3B*

N738S mutations (FD)**.** Lineage affiliations of the colonies are as in **Fig. 1d**. Numbers next to the bars indicate the number of colonies analyzed.

e) Bar graph showing the lineage affiliation of colonies from Lin^-CD34^+ normal cord blood (CB) cells (n=5 biologically independent samples) and $CD34^+$ BM cells in the CR sample of patient #201-022. Numbers next to the bar indicate the number of colonies produced per 100 plated cells. The GM:E (granulocyte-macrophage:erythroid) ratio of colonies and the 95% confidence interval for the GM:E ratio in normal BM are shown.

Figure 3. Enasidenib induces differentiation from an ancestral IDH2 mutant clone.

All data shown refer to samples from patient #201-023.

a) Heat map of targeted re-sequencing of mutations (rows) in single cells (columns, n=63 cells) from flow-sorted BM populations isolated pre-ENA and at CR which are shown together. Clonal identification of each cell is shown below the heat map and the key to mutations is denoted by letters on the right. Mutation detection key: red=detected; blue=not detected; white= sequencing failed.

b) Clonal structure of the AML sample based on single cell genotyping (SCG). Number next to a clone indicates the number of cells identified in that clone (data from a). The most likely clonal structure is shown in solid arrows with alternatives in dotted arrows. (*) indicates genotype “A” or “SIAR”, which were each detected in only 1 cell. § indicates genotype “AS” with ADO of an *IDH2* allele in 2/3 cells. Ø “SI” with ADO of the *ASXL1* allele in 3/12 cells. See also Supplementary Fig. 12a.

c) Clonal composition in different immunophenotypic compartments pre-ENA and at CR. Number of cells studied are indicated.

d) Clonal contribution (vertical bars) to immunophenotypic stem, progenitor, myeloid precursor and terminal mature GM populations in patient samples pre-ENA and at CR (horizontal bars). Data is from SCG except for mature GM population at CR, where the flow-sorted cell population was genotyped (*). Normal BM is shown for comparison of immunophenotypic populations.

e) Clonal contribution to colonies grown from CR sample (percentage of genotyped, individually picked colonies). Key to mutations detected are as in (b). Numbers next to the bars indicate the numbers of colonies analyzed. Lineage affiliations are as in **Fig. 1d**.

f) Lineage affiliation of colonies from BM $CD34^+$ cells purified from CR sample compared with normal CB (as in **Fig. 2e**).

Figure 4. Enasidenib induces differentiation from a terminal IDH2m clone.

All the data here are from patient #201-011.

a) Heat map of targeted re-sequencing of mutations (rows) in single cells (columns, n=110 cells) from flow-sorted BM populations pre-treatment and CR which are shown together. The key is as in **Fig. 3a**.

b) Clonal structure of the AML sample based on SCG. The key to the panel is as in **Fig. 3b**. * marks the genotype "DIA" where ADO was detected in 6/7 cells. Ø denotes genotype "DId". No heterozygous germline SNPs were available in the *ASXL1* gene. Estimated ADO frequency of the *ASXL1* allele was 12.1%. See also Supplementary Fig. 12c.

c) Clonal composition in different immunophenotypic compartments pre-ENA and at CR, as in **Fig. 3c.**

d) Clonal contribution (vertical bars) to immunophenotypic BM haematopoietic populations in patient samples pre-ENA and at CR (horizontal bars). Data is from SCG except for mature GM population pre-ENA, where the flow-sorted cell population was genotyped (*).

e) Clonal contribution to colonies grown from CR sample (percentage of genotyped, individually picked colonies) as in **Fig. 3e**.

f) Lineage affiliation of colonies from BM $CD34^+$ cells purified from CR sample compared with normal CB (as in **Fig. 2e**).

Figure 5. Mechanisms leading to relapse of enasidenib-treated patients.

a) Summary of mechanisms (rows) leading to relapse in 12 patients (columns). Selected mutations detected at relapse by WES (all patients except #104-021) or by Heme Panel bait capture sequencing (#104-021) are shown.

b) Longitudinal analysis of the percentage suppression of serum 2-HG concentrations prior to enasidenib treatment (pre-ENA), at best response (CR or PR) and at relapse in 14 patients with an *IDH2* R140 codon mutation.

c-d) Serum 2-HG levels and bone marrow blast percentages prior to enasidenib treatment (pre-ENA), at CR or CRp (complete remission without platelet recovery) during the course of treatment (C=cycle, D=day of treatment) and at relapse in patients #201-014 (c) and #201-022 (d).

e-f) Serial mutation analyses in flow-sorted blasts prior to enasidenib treatment (pre-ENA) and at relapse in patients #201-014 (e) and #201-022 (f).

Figure 6. Relapse post-enasidenib occurs through clonal evolution/selection.

a) Patient #104-021: Heat map of targeted re-sequencing of mutations (rows) in single cells (n=214 cells, columns) from flow-sorted BM populations pre-treatment and at relapse which are shown together. The key is as in **Fig. 3a**.

b) Clonal structure of patient #104-021 based on SCG. The key to the panel is as in **Fig. 3b**. Boxes in dotted red lines highlight clones which are only detected at relapse.

c) Clonal composition in different immunophenotypic compartments pre-ENA and at relapse, as in **Fig. 3c.**

d) Clonal contribution (vertical bars) to immunophenotypic BM haematopoietic populations in patient samples pre-ENA and at relapse (horizontal bars). Data is from SCG.

e) Patient #201-011: Heat map of targeted re-sequencing of mutations (rows) in single cells (n=87 cells, columns) from flow-sorted BM populations at relapse. The key is as in **Fig. 3a**.

f) Clonal structure of patient #201-011 at relapse. * indicates 6 cells with genotype “DIA” where we detected ADO in 4/5 cells in the *DNMT3A* allele. Ø denotes “DId”. The estimated ADO frequency of the *ASXL1* allele was 12.1%. § indicates 6/7 “DIXF” cells where there was ADO for the *DHX15* R222G mutant allele. See also Supplementary Fig. 12c. Boxes in dotted red lines as in (b).

g) Clonal composition in different immunophenotypic compartments at relapse, as in **Fig. 3c.**

h) Clonal contribution (vertical bars) to immunophenotypic BM haematopoietic populations in patient samples at relapse (horizontal bars). Data is from SCG.

Online Materials and Methods

Please see also the Life Sciences Reporting Summary

Patient samples

Bone marrow (BM) or blood samples from normal donors and AML patients were obtained with informed consent and collected by research ethics committee-approved Biobanks (MDSBio Study, MREC 06/Q1606/110, Oxford Musculoskeletal Biobank, MREC 09/H0606/11: South Central Oxford C REC), Gustave Roussy (Department of Clinical Hematology and Drug Development Department (DITEP), Gustave Roussy, Villejuif) and MSKCC Biobanks. Cytogenetic analyses were performed in clinical laboratories. Mononuclear cells (MNCs) were isolated by Ficoll density gradient. MNCs were viably frozen in 90% FCS/10% DMSO in liquid nitrogen.

Measurement and analysis of 2-hydroxyglutarate (2-HG)

Serum samples were collected within 28 days before the first dose of enasidenib ('screening') and/or pre-dose on day 1 of each treatment cycle. 2-HG concentration was determined by liquid chromatography tandem mass spectrometry (Covance, Inc USA according to their validated method). Baseline 2-HG was either the average of the screening sample and pre-dose cycle 1 sample, or either sample if both were not available. Percentage suppression of 2-HG was determined by comparing the lowest level of 2-HG observed on-treatment to baseline.

Hematopoietic cell immunophenotyping

Frozen BMMNCs from normal donors or AML samples were washed with Iscove's Modified Dulbecco's Medium (Thermo Fisher Scientific, UK), 10% fetal bovine serum (Sigma, UK) and 1mg/ml bovine pancreatic DNAse I (Sigma, UK). Cells were stained for flow cytometry with antibodies in Supplementary Table 8. Analysis was carried out on either BD LSR

727 Fortessa or BD FACSAria Fusion (Becton Dickinson, Oxford UK). Antibodies in the lineage
728 (Lin) depletion are: anti-CD2,CD3,CD4,CD8a,CD10,CD19,CD20 and CD235a. 7-
729 aminoactinomycin-D (7AAD, Becton Dickinson, UK) was used as a live/dead stain.
730 Hematopoietic stem/progenitor cells were defined as subsets of Lin^-CD34^+ and myeloid
731 precursor as $Lin^-CD34^-CD117^+$ as previously described[21]. Terminally mature myeloid cells
732 were defined as $Lin^-CD34^-CD117^-$.

733 **Mutational analysis by FoundationOne® Heme Panel**

734 Analysis of samples in **Fig. 1a** by FoundationOne® Heme panel was conducted by
735 Foundation Medicine, Inc. Nucleic acid libraries were prepared from DNA and RNA extracted
736 from fresh patient BM samples and captured using custom bait-sets targeting 405 cancer-
737 related genes by DNA-sequencing (DNA-seq), and 265 frequently rearranged genes by
738 RNA-sequencing (RNA-seq). Genes included in this analysis encode known or likely targets
739 of therapies, either approved or in clinical trials, or are otherwise known drivers of
740 oncogenesis published in the literature[52].

741 **Mutational analysis by Fluidigm Access Array**

742 Selected samples from **Fig. 1a** and **Supplementary Table 2** was performed using highly
743 multiplexed PCR-based targeted re-sequencing with a custom panel of 373 amplicons
744 covering areas of high frequency AML mutations in 35 genes, using the Fluidigm Access
745 Array platform as previously described[6].

746 **Mutational analysis by whole exome sequencing (WES).**

747 Genomic DNA from flow-sorted AML blasts or CD3-positive cells (germline control) was
748 purified with Allprep DNA/RNA mini or micro Kits (Qiagen, France). After exome capture with
749 SureSelect V5 Mb All Exon kit (Agilent, Les Ulis, France), paired-end 100 bp sequencing
750 was performed on HiSeq2000 (Illumina, Paris France). Read alignment to hg19 reference
751 genome was performed using the BWA algorithm, v0.7.10 with corrections using GATK
752 (v3.3.0) after removal of PCR duplicates. Variant detection was carried out with VARSCAN
753 (v2.3.7). Somatic variants (**Supplementary Table 2**) were selected using the following
754 criteria: minimum depth: 8x, VAF>10% in AML blasts and lower than 10% in germline

control, and p-value <0.001. All variants were manually inspected using IGV (v2.3) software. Artifactual variants from DNA oxidation where read pair orientation bias was observed (i.e. predominant F2R1 orientation for C to A variations or F1R2 for G to T variations) were filtered out. Median depth at the positions reported in the **Supplementary Table 2** was 121 (range: 19-843).

Selection of mutations for targeted re-sequencing in populations and single cells.

On average 23 somatic mutations were detected per AML sample by WES. We selected mutations for further validation by targeted re-sequencing and SCG based on the following criteria: 1) known recurrent mutations in AML, 2) non-recurrent mutations in genes commonly mutated in AML. In addition, mutations not meeting above criteria, but where the VAF varied by at least 5% between sequential samples in the same patient were of interest as these may be markers of clonal shifts. Where multiple mutations had similar VAFs and showed similar patterns of change in VAFs in sequential samples, a representative mutation was selected. This is illustrated in the example from patient #201-011 (Supplementary Figure 11a). Mutations which were not validated by targeted re-sequencing were excluded in subsequent data analysis. Chromosomal loss of heterozygosity detected by WES (or by karyotyping) was examined using germline single nucleotide polymorphisms (SNP) present in the affected chromosomal region.

Mutational analysis by targeted re-sequencing

Mutations detected by targeted re-sequencing in hematopoietic cell populations are in **Supplementary Table 3**. Average and range of read depths for each mutation is shown in **Supplementary Table 4**. DNA was extracted (DNeasy Blood and Tissue extraction kit, #69506 Qiagen Manchester UK) from bulk and flow-sorted cells from patient samples. Where material was limiting, whole genome amplification (WGA, RepliG, Qiagen, UK)) was performed. Targeted PCR was performed using high Fidelity Phusion Taq polymerase (NEB, UK) or KAPA2G Multiplex DNA Polymerase (KAPA Biosystems, UK) with 10ng of gDNA. Primers used are in **Supplementary Table 7.** A second PCR reaction added Illumina barcodes and sequencing oligonucleotides prior to sample purification, quantitation, pooling

and library preparation for sequencing on Illumina MiSeq (Illumina, Saffron Walden, UK). Raw data (average depth ~996x) was aligned using Stampy (v1.0.20)[53]. A minimum sequencing depth of 100 was set as a threshold for inclusion of data for analysis. >94% of reads had Phred scores of >30. VAF was obtained using the Unix 'grep' (**g**lobally search **re**gular expression and **p**rint) command line.

Mutant *IDH2* variant allele frequency by quantitative PCR.

mIDH2 VAF was assessed in gDNA extracted from flow-sorted patient blood $CD14^+$ monocytes, $CD16^+$ neutrophils, or polymorphonuclear neutrophils (Ficoll gradient purification) at various time points during enasidenib treatment. Quantitative SNP assay PCR (12.5ng DNA per test) was performed using TaqMan® Universal PCR Master Mix (Applied Biosystems, France), TaqMan® probes (specific for either IDH2 wild type (FAM) or mutated R140Q (VIC) alleles (rs121913502, Applied Biosystems, France)). PCR was performed on an ABI 7500 Fast Real-Time PCR analyzer (Applied Biosystems, France) with cycling conditions: initial 1min at 60°C, 10min at 95°C, followed by 40 cycles of 15sec at 95°C and 1min at 60°C; and then 1min at 60°C.

Single cell genotyping

Mutations interrogated by SCG are in **Supplementary Table 3**. Single cells were flow-sorted into 96 well plates containing 2µl of phosphate buffered saline. WGA was carried out using Single Cell RepliG kit (Qiagen, Crawley UK). Briefly, following cell lysis, alkali denaturation and neutralisation, a master mix containing Phi29 polymerase, dNTPs and random oligonucleotide primers was added. WGA was carried out at 30^0C for 8 hours followed by heat inactivation. Diluted (1:20) amplified DNA was used in single or multiplex PCR using primers relevant to the sample and high Fidelity Phusion Taq polymerase (NEB, UK) or KAPA2G Multiplex DNA Polymerase (KAPA Biosystems, UK). Barcoding and sequencing oligonucleotides were added by PCR and sequencing performed on Illumina MiSeq (Illumina, Saffron Walden, UK). ~94% of reads had Phred scores of >30. A threshold of 50 reads was set for analysis inclusion. VAF thresholds for determining detection of mutations were determined by genotyping 48 single cells derived from normal bone marrow, and set at

the 95% confidence level (mean ± 1.96 x standard error of mean (SEM); i.e. <5% chance of false positive, **Supplementary Table 6**).

Imputation of clonal structures using bulk VAFs

The most common method used to impute clonal structure is based on the assumption that the most abundant mutation resides in the earliest occurring ancestral clone. This method may be applicable to samples with linear clonal structures but it may not be able to accurately resolve more complex or branching clonal structures. Longitudinal bulk genotyping data may offer additional information, particularly where there is evidence of clonal selection or evolution.

Putative clonal structure is first solved for each sample independently using bulk VAF data based on the rules below. In samples where there was no colony or single cell (SC) genotyping, longitudinal sampling (pre-ENA, best response and relapse) can provide additional information on the likely clonal structure of that patient. In the absence of colony or SCG data, bulk VAFs were used to estimate the size of the most likely clones in samples. In samples where there is associated colony and/ or single cell (SC) genotyping, the clonal structure was re-drawn based on these data, which provide a higher confidence structure with some resolution of intermediate clones. Once this clonal structure is solved, bulk VAF was used to estimate the sizes of clones in samples.

Sequence of acquisition of mutations can be imputed from bulk genotyping data, using VAF as an estimate of clonal contribution (Supplementary Fig. 11b). Mutations are first ranked according to VAF: in these examples, V_A is highest, V_D is lowest.

Factors which may cause data error and bias include limited cell equivalent representation in extracted genomic DNA from small cell numbers, bias present in whole genome amplified material and PCR bias (including sequencing bias). While we were unable to control for the first two factors, we could estimate standard error of our sequencing data. We performed technical replicate genotyping of 19 unsorted BMMC populations and obtained the standard error of mean (SEM) from VAFs from each mutation. In total, 142 standard error values

were obtained, and the average SEM was 1.9% (range 0.0-20.2%), with a 95% confidence interval upper limit of 2.47%. This limits our ability to reliably distinguish between clones varying in VAF of ~2.5% (~5% of cells if mutations were heterozygous), and we were not able to impute sequence of acquisition of mutations in population genotyping with less than 2.5% difference in VAF between them. Where three or four mutations have VAF within 2.5% of each other, the average VAF of the cluster is taken as the VAF of all mutations in that cluster (Supplementary Fig.11c).

Interpreting VAFs and cellular representation in the context of loss of heterozygosity or hemizygosity.

We detected multiple occurrences of loss of heterozygosity (LoH, e.g. copy-loss chromosomal deletions or copy-neutral uniparental disomy) and mutations, which were on the X chromosome in male patients (hemizygosity). There is complexity in interpreting bulk VAFs due potential mix of cells with or without LoH within a bulk population. Notwithstanding this caveat, we used the simple models set out below to help interpret VAFs in different contexts. For somatic heterozygous variants (somatic mutation or germline polymorphism) in autosomal chromosomes the estimated percentage cellular representation is 2xVAF% (Supplementary Fig. 11d). Heterozygous variant and chromosomal deletion resulting in copy-loss LoH in autosomal chromosomes is illustrated in Supplementary Fig. 11e. Here, there is a non-linear relationship between VAF and cellular representation (Supplementary Fig. 11f). The formula we used to estimate cellular representation was: % cellular representation= $[-2.777 \times (\text{VAF ratio})^2] + (6.145 \times \text{VAF ratio}) - 2.373$. In heterozygous variants and copy-neutral LoH (e.g. uniparental disomy) in autosomal chromosomes, percentage cellular representation is 100% -(2xVAF%) (Supplementary Fig. 11g). In X-linked variants in male subjects in sex chromosomes: percentage cellular presentation is the same as the VAF% (Supplementary Fig. 11h).

Determination of clonal structures using single cell genotyping

Each single cell was assessed for detection or non-detection of mutations in that patient sample by amplicon sequencing of DNA subject to whole genome amplification. A minimum

coverage of 30x across an amplicons was required for a amplicon to be called. We assigned the most likely sequence of acquisition of mutations based on the genotype identified in cells. For example, where mutations A, B, C, D and E were identified in a sample, discrete cells with genotypes A, AB, ABC, ABD, ABCD and AE may be called. In most cases the sequence of acquisition, e.g. A->AB, is clear. However, the sequence of acquisition of mutations during the transition for example, from AB to ABCD may not be clear due to allelic drop out (ADO) i.e. the sequence of acquisition may be AB -> ABC -> ABCD or AB-> ABD-> ABCD. In such cases, intermediate genotypes represented by most cells may be more likely to be true. In all cases, models of clonal structures which require the least number of discrete mutational steps required are represented[54], although alternative structures, including ones where the same mutation is acquired twice, are possible. Once the most likely clonal structure is established, cells where there was failure to amplify a locus that did not alter the assignment of a mutational complement (e.g. an early mutation in the hierarchy) were included in the final analysis.

Allele Drop Out Estimation (ADO)

ADO can be measured for by two methods. First, ADO can be determined by determining the phase of germline SNPs near mutations. For patients #201-023 and #201-011, we genotyped germline SNPs which were either in-phase (i.e. on the same allele as) with a mutation or out of phase (i.e. on the opposite allele).

In-phase SNPs were rs6597996 and rs11246258, *DEAF1* N372K mutation, patient #201-011. Out-of-phase SNPs were: (i) rs4911231, *ASXL1* G646fs mutation, patient #201-023; (ii) rs2276598, *DNMT3A* R598X, patient #201-011; (iii) rs7657364, *DHX15* R222G, patient #201-011. The SNPs were situated between 157 bases and 4 kilobases from the mutations. The threshold VAF for ascertaining dropout in these SNPs was <2% (homozygous reference) or >98% (homozygous variant).

In patient #201-023 (**Fig. 3a-b**) in 2/3 cells with the "AS" genotype there was ADO of one of the *IDH2* alleles (Supplementary Fig. 12a, left) and in 2/12 cells with the genotype "SI" there was ADO in the *ASXL1* allele (Supplementary Fig. 12a, right).

Our analysis also showed that in patient #201-011 *DNMT3A* R598X and R736C mutations are on different alleles and the R736C mutation is in phase with rs2276598 (Supplementary Fig. 12b).

By studying both VAFs of the SNP rs2276598 and the R736C mutation in cells with genotype "DIA" in patient #201-011 where ADO may have occurred we determined that in 6/7 cells at CR, ADO of the allele that harboured the R598X mutation had occurred (Supplementary Fig. 12c left). Where the SNP did not amplify, the VAF of R736C mutation was informative. Similarly, in the same patient at relapse, 5/6 "DIA" cells at relapse had ADO of the R598X allele (Supplementary Fig. 12c center). We also determined that in 6/7 cells with the "DIXF" genotype at relapse there had been ADO of the allele harbouring the *DHX15* R222G mutation (Supplementary Fig. 12c, right).

An alternate method to determine ADO more globally is to study the frequency with which a variant is called homozygous (either reference or alternative) when it should be heterozygote. We analysed 6 SNPs in 5 genes (*ASXL1*, *IDH2, DNMT3A, DEAF1* and *DHX15*) in 402 single cells from 2 patients (#201-011 and #201-023) known to be heterozygous in the germline (confirmed by genotyping population of flow sorted T cells from the patients). Mean VAF was 49.1% for all 6 SNPs with a near-symmetrical distribution of VAFs across these single cells ranging from 0-100% (Supplementary Fig. 12d). Frequencies of homozygous reference (VAF≤1%) or variant calls in the 402 cells (VAF≥99%, thresholds based on analysis of known homozygous SNPs in 237 cells) were 15.9% (64 cells/402 cells) and 15.2% (61 cells/402 cells) respectively (Supplementary Fig. 12d).

Next, if we assume that mutations in patients were heterozygous (i.e. in cases where there is was no data to support uniparental disomy or copy number loss) we asked what was the frequency with which mutations were called homozygous (VAF≥99%) (presumably due to

ADO). Across the 23 mutations assessed using this method, the average ADO rate of wild type allele was 10.36% (SD 5.7%, Supplementary Fig. 12e). However, we found variation in ADO rates between different patients, even at the same mutation (e.g. *IDH2* R172K), suggesting that ADO is affected by factors additional to that of the activity of the Phi21 polymerase. Where possible we have used gene-specific germline SNPs, or alternatively used sample and mutation specific ADO estimated by the 'homozygous mutant' method for our analyses.

Digital Droplet PCR

We confirmed the VAFs detected by next-generation sequencing (NGS) using digital droplet PCR (ddPCR) in 17 amplicons and 113 sorted multi-cell AML populations from 5 patients using the BIORAD platform as previously described[21]. There was good correlation between VAF values obtained using these two methods (R^2= 0.974,). There was one AML variant (DHX15 R222G) where NGS gave an unexpectedly high VAF in single normal BM MNCs (where the mutation was found to be absent in the bulk normal BM sample). Detection of this variant in normal and AML were therefore carried out using ddPCR which showed presence of the mutation in AML bulk and single cells, but confirmed its absence in normal bulk and single cells.

Whole transcriptome sequencing (RNAseq) and analysis of alternative splicing events

Copy DNA libraries were prepared using extracted RNA from AML blast cells flow-sorted from re- and post-relapse samples from patients #201-011 and #201-013. cDNA libraries were prepared for sequencing with tagmentation and indexing using Illumina Nextera Sample Preparation kit (Illumina, Saffron Walden, UK). RNA-seq data were generated as 75 bp paired-end unstranded Illumina reads. Reads were aligned using STAR(v2.4.0.1)[55] to the human genome (GRCh37) with default parameters. On average alignment was 96.7% (range: 95.5-97.4%) with an average of $139x10^6$ (range: $116x10^6$-$169x10^6$) mapped reads per sample. Differentially spliced events (DSEs) for the wild type (pre-relapse) and post-relapse with spliceosome gene mutations analysed as paired samples, were identified[56] using Mixture of Isoforms (MISO v0.5.4) using default parameters. An event is termed as

differentially spliced if the Bayes Factor (BF) ≥ 10, $|\Delta PSI| > 0.2$ where PSI is 'percentage spliced in', and the event is supported by ≥ 10 reads. DSEs are classified included or skipped spliced exons (SE), alternative 3'/5' splice sites (A3SS, A5SS), mutually exclusive exons (MXE) or retained introns (RI).

Colony assays

25-250 cells were plated in duplicate in 1.2ml of MethoCult GFH4435 (StemCell Technologies, Manchester, UK). AML patient samples were assayed with added Enasidenib (1μM). The rest of the procedure was as previously described[20].

Statistical Analysis

Where applicable, statistical analyses were performed using with GraphPad Prism software (v7.02) using statistical methods noted in figure and table legends.

References

6. Craddock, C.F., *et al.* Outcome of Azacitidine Therapy in Acute Myeloid Leukemia Is not Improved by Concurrent Vorinostat Therapy but Is Predicted by a Diagnostic Molecular Signature. *Clin Cancer Res* (2017).

20. Goardon, N., *et al.* Coexistence of LMPP-like and GMP-like leukemia stem cells in acute myeloid leukemia. *Cancer Cell* **19**, 138-152 (2011).

21. Quek, L., *et al.* Genetically distinct leukemic stem cells in human CD34- acute myeloid leukemia are arrested at a hemopoietic precursor-like stage. *J Exp Med* **213**, 1513-1535 (2016).

52. He, J., *et al.* Integrated genomic DNA/RNA profiling of hematologic malignancies in the clinical setting. *Blood* **127**, 3004-3014 (2016).

53. Lunter, G. & Goodson, M. Stampy: a statistical algorithm for sensitive and fast mapping of Illumina sequence reads. *Genome Res* **21**, 936-939 (2011).

54. Potter, N.E., *et al.* Single-cell mutational profiling and clonal phylogeny in cancer. *Genome Res* **23**, 2115-2125 (2013).

973 55. Dobin, A.*, et al.* STAR: ultrafast universal RNA-seq aligner. *Bioinformatics* **29**, 15-21
974 (2013).
975 56. Katz, Y., Wang, E.T., Airoldi, E.M. & Burge, C.B. Analysis and design of RNA
976 sequencing experiments for identifying isoform regulation. *Nat Methods* **7**, 1009-1015
977 (2010).

978

Figure 1

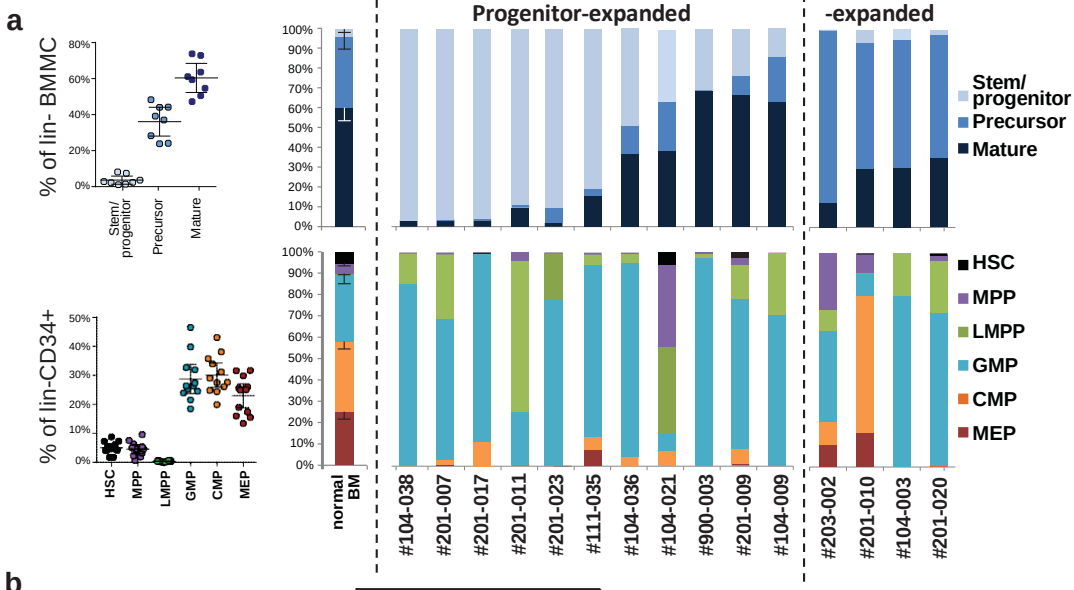
a
% of lin- BMMC
Stem/ progenitor
Precursor
Mature
% of lin-CD34+
HSC
MPP
LMPP
GMP
CMP
MEP
normal BM
Progenitor-expanded
Precursor -expanded
#104-038
#201-007
#201-017
#201-011
#201-023
#111-035
#104-036
#104-021
#900-003
#201-009
#104-009
#203-002
#201-010
#104-003
#201-020
Stem/ progenitor
Precursor
Mature
HSC
MPP
LMPP
GMP
CMP
MEP

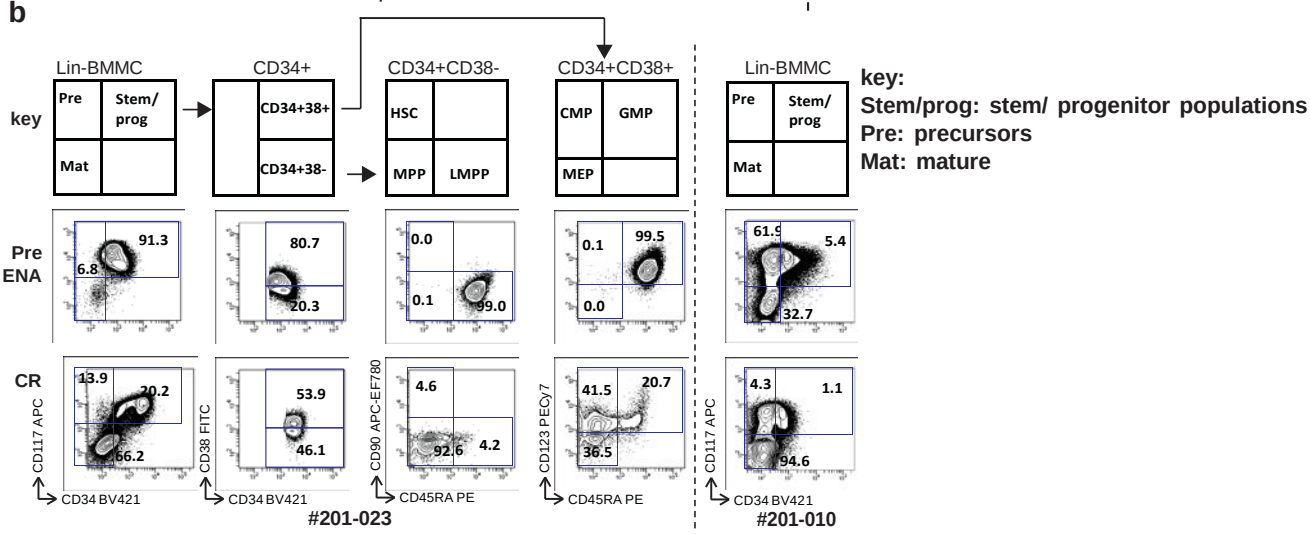
b
key
Lin-BMMC
Pre
Stem/ prog
Mat
CD34+
CD34+38+
CD34+38-
CD34+CD38-
HSC
MPP
LMPP
CD34+CD38+
CMP
GMP
MEP
Lin-BMMC
Pre
Stem/ prog
Mat
key:
Stem/prog: stem/ progenitor populations
Pre: precursors
Mat: mature
Pre ENA
CR
91.3
6.8
80.7
20.3
0.0
0.1
99.0
0.1
99.5
0.0
61.9
5.4
32.7
13.9
20.2
66.2
53.9
46.1
4.6
92.6
4.2
41.5
20.7
36.5
4.3
1.1
94.6
CD117 APC
CD34 BV421
CD38 FITC
CD34 BV421
CD90 APC-EF780
CD45RA PE
CD123 PECy7
CD45RA PE
CD117 APC
CD34 BV421
#201-023
#201-010

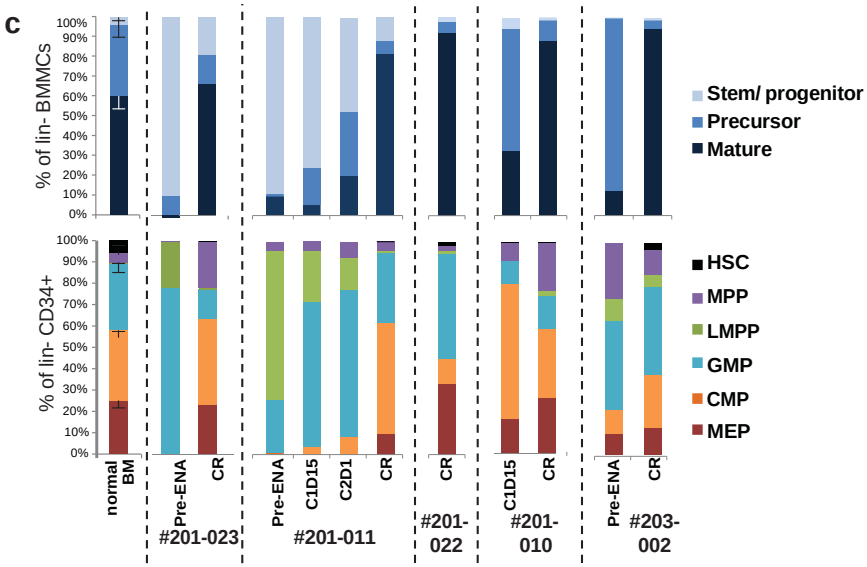
c
% of lin- BMMCs
% of lin- CD34+
Stem/ progenitor
Precursor
Mature
HSC
MPP
LMPP
GMP
CMP
MEP
normal BM
Pre-ENA
CR
#201-023
Pre-ENA
C1D15
C2D1
CR
#201-011
CR
#201-022
C1D15
CR
#201-010
Pre-ENA
CR
#203-002

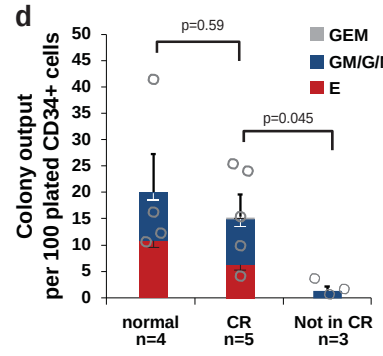
d
Colony output per 100 plated CD34+ cells
p=0.59
p=0.045
GEM
GM/G/M
E
normal n=4
CR n=5
Not in CR n=3

Figure 2

a Clonal origin of complete remission response to Enasidenib

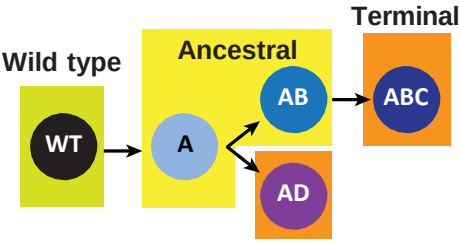

b

Patient ID	#201-022	#201-023	#201-010	#201-011	#201-006	#201-027
Wild type	■					
Ancestral		■				
Terminal			■	■	■	■

c

#201-022		IDH2 R140Q (I)	PEX26 P118S (P)	FEZ2 S208T (F)	DNMT3B N738S (D)	ZCCHC1 T712M (Z)	NPM1 L135 delins LLSIFKG (N)	ELMO3 R725Q (E)
VAF	Pre- ENA AML blasts	36.00%	25.45%	24.96%	23.20%	22.72%	22.17%	1.83%
	CR PBMNCs	0.24%	1.00%	1.23%	1.61%	0.58%	0.12%	0.31%

d

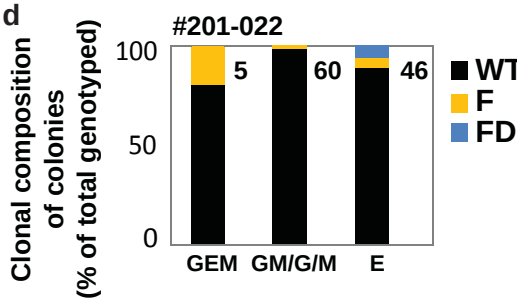

e

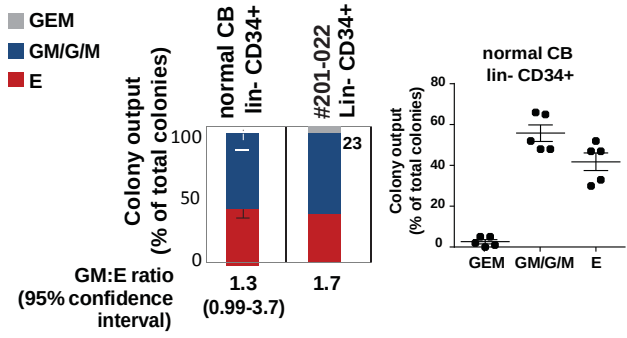

Figure 3

#201-023

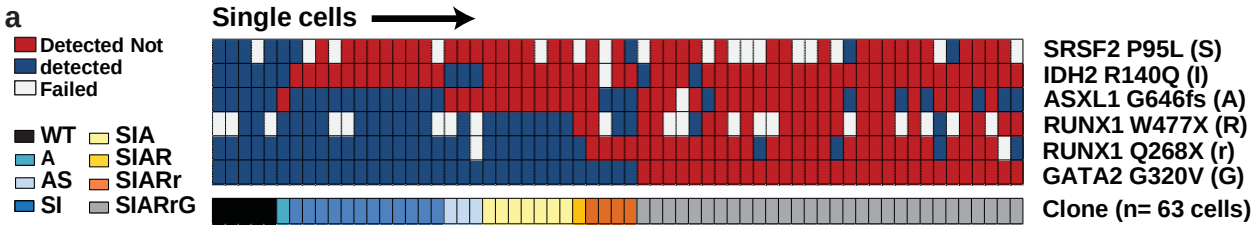

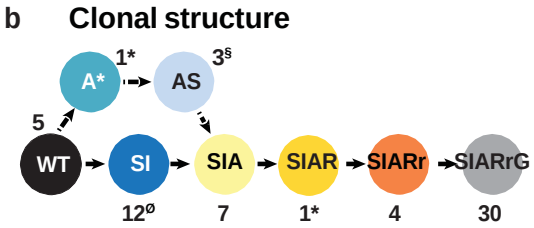

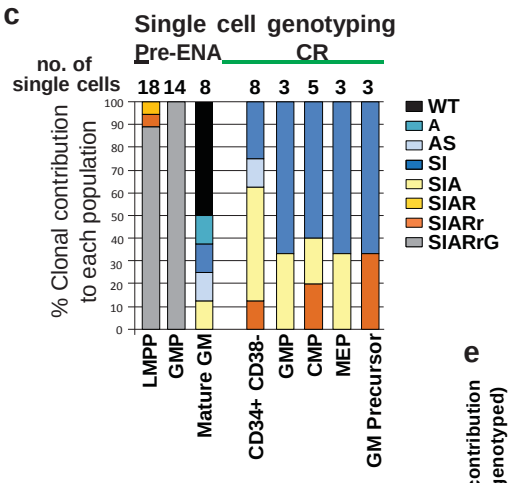

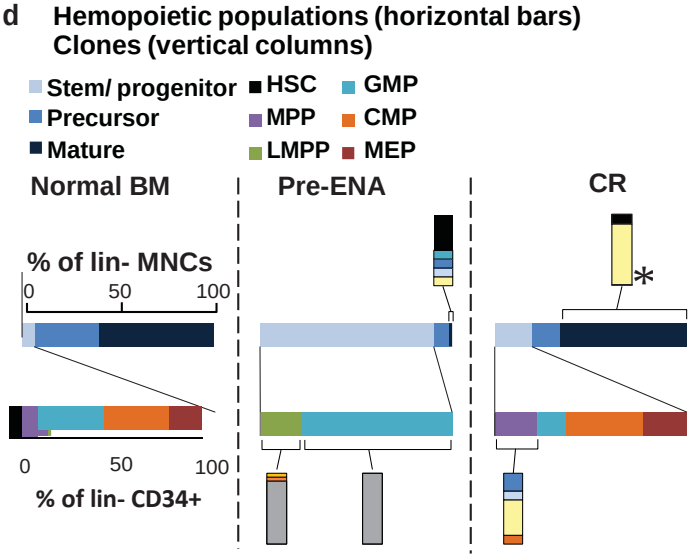

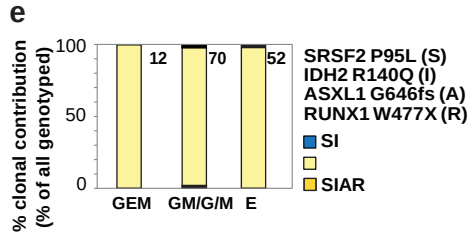

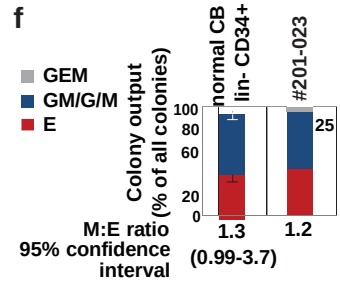

Figure 4
#201-011

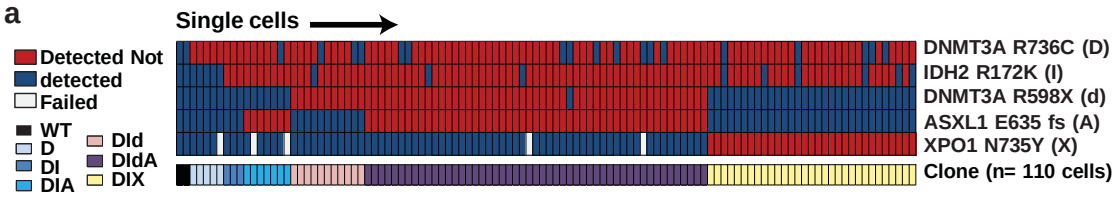

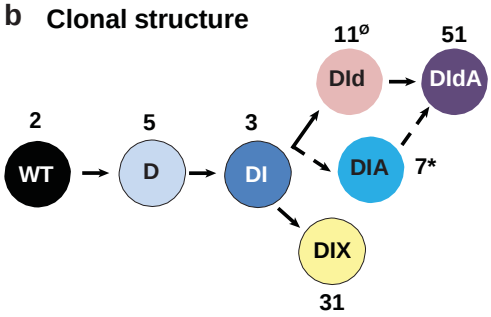

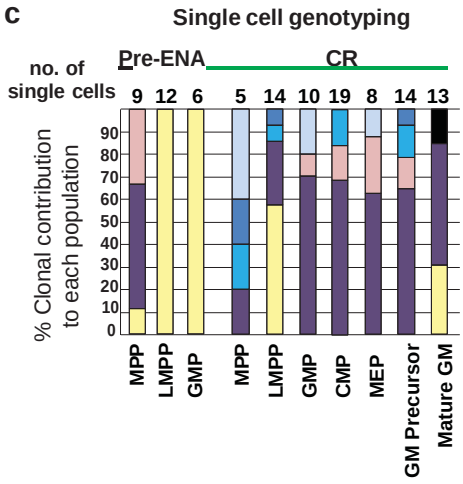

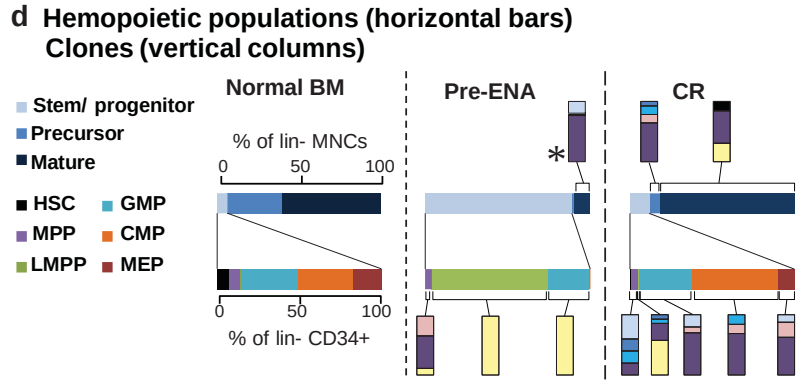

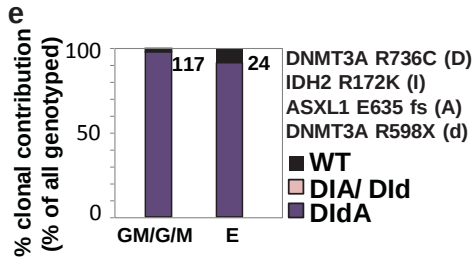

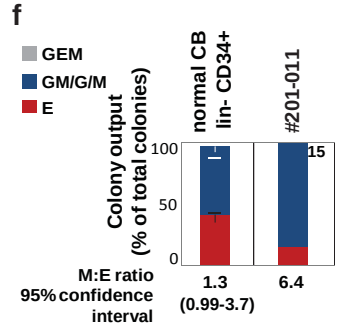

Figure 5

a

Patient ID	#201-014	#201-022	#104-021	#201-013	#201-004	#201-006	#201-010	#201-007	#201-019	#201-003	#201-011	#201-012
IDH1	IDH1 R132C	IDH1 R132H										
cytokine receptor signalling			CSF3R T618I	FLT3 D835A	FLT3 ITD			FLT3 I867M				
haematopoietic transcription factor	RUNX1 F416 Gfs*135			BCL11A N391K	GATA2 N317S/ L321R	RUNX1 T188 Hfs*25						
genes implicated in spliceosome function				DDX1 G699A							DHX15 R222G	
other genes recurrently mutated in haematopoietic cancer		ELMO3 R725Q	NFKB1 M216I	BCOR R1375W	BRCA2 A2643V				SCN3A R28H	AKAP8L D89N	DEAF1 N372K	
				CACNA1G G663R	CBLsplice acceptor				SETD1B A1054 delinsAE	PLCL1 A985V		
				UGT2B10 Y16*								
other genes recurrently mutated in other cancer				SLC18A3 W105*			IL17A P130S	MTUS Q835H		DOM3Z Y92*		
deletion chr 7q												

b

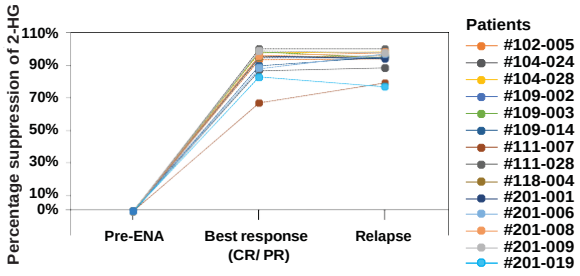

c #201-014

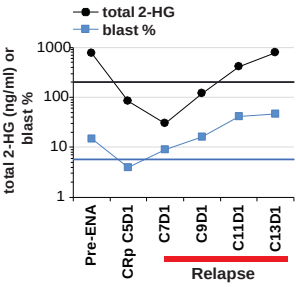

e #201-014

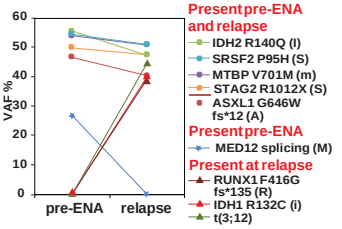

d #201-022

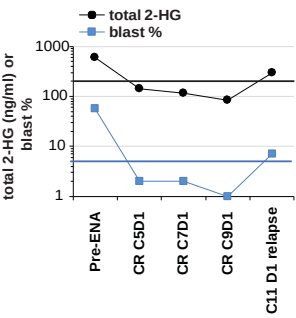

f #201-022

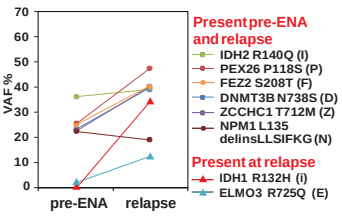

Figure 6

#104-021

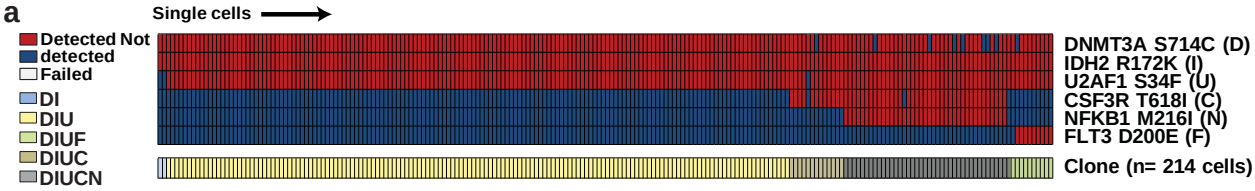

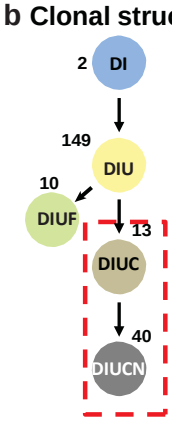

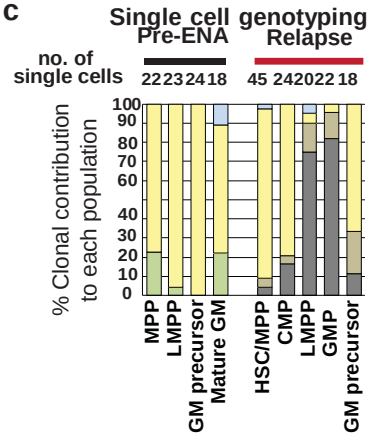

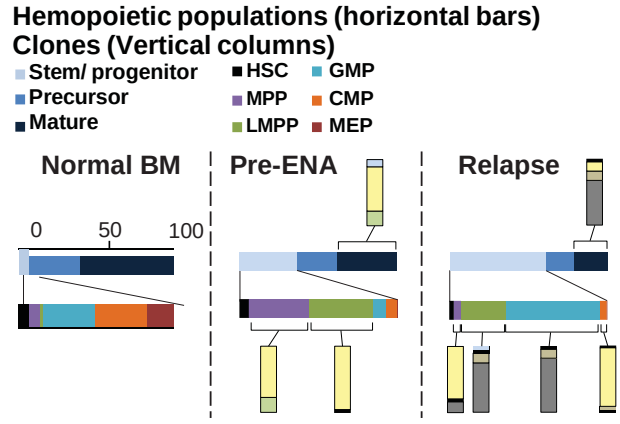

#201-011 (Relapse)